Ukrainian Journal of Remote Sensing
journal homepage: www.ujrs.org.ua

https://doi.org/10/36023/ujrs.2022.9.2.212

UDC 621.3:004.932

Prediction of Parameters in Optimal Operation Point for BPG-based Lossy Compression of Noisy Images

B. V. Kovalenko[1]*, V. V. Lukin[1], S. S. Kryvenko[1], V. V. Naumenko[1], B. Vozel[2]
[1] Department of Information and Communication Technologies, National Aerospace University, 61070 Kharkiv, Ukraine
[2] IETR, UMR CNRS 6164, University of Rennes 1, 22305, Lannion, France

Lossy compression of images corrupted by noise has several peculiarities. First, a specific noise filtering effect is observed. Second, optimal operation point (OOP) can be observed, i.e. such coder parameter (e.g., quantization step) value can exist that quality of compressed image calculated with respect to noise-free image can be better compared to quality of uncompressed (original noisy) image. If OOP exists, it is worth compressing a given image in OOP, if no, other recommendations on coder parameter setting are reasonable. Since noise-free image is not available in practice, it is not possible to determine does OOP exist and what is image quality in it. In this paper, we show that OOP existence for several quality metrics can be predicted quite easily and quickly for grayscale images corrupted by additive white Gaussian noise and compressed by better portable graphics (BPG) encoder. Such a prediction is based on analysis of statistics of discrete cosine transform (DCT) coefficients calculated for a limited number of 8x8 pixel blocks. A scatter-plot of metric improvement (reduction) depending upon these statistics is obtained in advance and prediction curve fitting is performed. Recommendations on encoder parameter setting for cases of OOP absence are given.
Keywords: image lossy compression; optimal operation point; quality prediction; noise; discrete cosine transform
© B. V. Kovalenko, V. V. Lukin, S. S. Kryvenko, V. V. Naumenko, B. Vozel. 2022

1. Introduction

Images of different origin are widely used in numerous applications, e.g., remote sensing (Aiazzi et al., 2012), medical diagnostics (Braunschweig et al., 2009), advertising (Bataeva et al., 2012), non-destructive control (Mahanti et al., 2021), everyday life (Zappavigna et al., 2016). The main tendencies observed in recent years in imaging deal with rapid increase of image number and image size (Khorram et al., 2016). This causes problems in image processing, storage, transmission, classification (Chi et al., 2016 and Ma et al., 2015). The problems in storage and transmission of imaging data can be solved by image compression (Hussain et al., 2018; Tao et al., 2018; Doss et al., 2020; Penna et al., 2007).

As it is known, image compression techniques can be divided into two main groups – lossless and lossy (Hussain et al., 2018 and Sayood et al., 2017). Lossless compression does not lead to introducing distortions into images (data) but has one drawback – the provided compression ratio (CR) is usually unacceptably small. Then, lossy compression occurs to be preferable since CR can be varied and controlled (Sayood et al., 2017 and Li et al., 2020). Meanwhile, CR increasing usually leads to worse quality of a compressed image and a reasonable compromise has to be found in each particular case (Tao et al., 2018; Pandey et al., 2020; Zabala et al., 2006; Christophe et al., 2011). This compromise depends on many factors: 1) what is the application of a considered image and how is it further processed (analyzed, interpreted) (Zabala et al., 2006 and Krivenko et al., 2019); 2) what is a coder (compression method) used and how easy is it to vary and control compression parameters; 3) what are properties (content, complexity) of an image to be compressed (Li et al., 2020 and Krivenko et al., 2019); 4) what are the main requirements to compression and their priority.

Concerning factor #1 – lossy compression should not result in too large degradation of image quality with respect to its visual perception by humans or classification or edge/object detection. The corresponding studies have been performed to predict just noticeable distortions (Bondžulić et al., 2021) or other measures of acceptable degradation of compressed images (Zabala et al., 2006 and Krivenko et al., 2011). Concerning factor #2 – different compression techniques employ different mechanisms of CR or compressed image quality variation and control. For example, JPEG2000 (Taubman et al., 2013) and SPIHT (Said et al., 1996) allow providing a desired CR (or bits per pixel (BPP)) with wide diversity of compressed image quality depending on its complexity (Li et al., 2020). In turn, a modern better portable graphics (BPG) coder (Yee et al., 2017 and Albalawi et al., 2016) uses the parameter Q that allows controlling peak signal-to-noise ratio (PSNR) between original and compressed images in wide limits (Kovalenko et al., 2021). This is a good quality attracting our attention just to this coder although PSNR is not an adequate metric in characterizing image quality (Zhai et

E-mail: b.kovalenko@khai.edu

al., 2020). Concerning factor #3 – for any coder, it is more difficult to compress more complex structure images with providing appropriate quality for a given CR. Moreover, noise presence in compressed images additionally complicates the task of image compression (Al-Shaykh et al., 1998; Chang et al., 1997; Zemliachenko et al., 2015; Naumenko et al., 2021). In this paper, we just consider the task of lossy compression of images corrupted by noise. Such a compression has certain peculiarities, in particular, noise filtering effect first discovered in (Al-Shaykh et al., 1998 and Chang et al., 1997) and possible existence of optimal operation point (OOP) that has been observed for many different compression methods based on either wavelets or discrete cosine transform (DCT). The main goal of our paper is to show that existence of OOP and compression parameters in it can be predicted for the BPG encoder with quite high accuracy. Finally, concerning factor #4, it is usually required to provide as high quality of compressed images as possible for a given CR, to carry out compression as quickly as possible and so on. Some of these requirements are contradictory and difficult to provide. In this paper, we concentrate on providing an appropriate quality of compressed images with as large CR as possible.

2. Used criteria and rate/distortion curves

A specific aspect of this paper is that we consider lossy compression of just noisy images. Noise appears in images due to many factors (Colom et al., 2014 and Chatterjee et al., 2010) and it can be visible or invisible. We concentrate on the case of visible noise that happens if PSNR of original image is less than a certain threshold (about 35 dB). Moreover, we focus on the simplest additive white Gaussian noise (AWGN) model (Chatterjee et al., 2010) leaving more complex noise models (Colom et al., 2014) for future studies.

According to this model, one has

$$I_{ij}^{noisy} = I_{ij}^{true} + n_{ij}, \quad (1)$$

where I_{ij}^{noisy} denotes the noisy *ij*-th pixel value, I_{ij}^{true} is the true *ij*-th pixel value, n_{ij} is the value of AWGN having zero mean and variance σ^2. Below we assume that noise variance is *a priori* known or pre-estimated (Colom et al., 2014 and Selva et al., 2021) with high accuracy.

The conventional metrics to characterize quality of original noisy image are mean square error (MSE) and peak signal-to-noise ratio (PSNR) calculated as

$$\mathrm{MSE}^n = \sum_{i=1}^{I}\sum_{j=1}^{J}\frac{\left(I_{ij}^n - I_{ij}^{true}\right)^2}{IJ}, \quad (2)$$

$$\mathrm{PSNR}^n = 10\log_{10}\left(\frac{255^2}{\mathrm{MSE}^n}\right) = 10\log_{10}\left(\frac{255^2}{\sigma^2}\right),$$

where *I*, *J* define image dimensions and it is supposed that the image is represented as 8-bit data. In such a case, noise, to be visible, should have variance about 20 for simple structure images (see an example in Fig. 1, a) and about 30…40 for complex structure ones (see examples in Fig. 1, b and 1, c) (Ponomarenko et al., 2015). This explains why we consider the values of noise variance larger than 40 in our simulations.

The quality of original (noisy) image can be also characterized by other metrics including visual quality ones. These can be, e.g., PSNR–HVS–M (Ponomarenko et al., 2007) or MS–SSIM (Wang et al., 2003). In particular,

$$\mathrm{PSNR-HVS-M}^n = 10\log_{10}\left(\frac{255^2}{\mathrm{MSE-HVS-M}^n}\right)$$

where MSE–HVS–M^n is defined in a set of 8x8 pixel blocks considering different sensitivity of human vision system (HVS) to distortions in different spatial frequencies as masking effect (Ponomarenko et al., 2007).

a b c

Fig. 1. Some examples of the test images: Frisco (a), Diego (b), and Fr01 (c)

We are more interested in other metrics and their dependences on compression parameters. In particular, consider the dependences $PSNR^c(Q)$ and $PSNR–HVS–M^c(Q)$ where these metrics are calculated for images compressed by BPQ with different Q and the corresponding original (noisy) images. Examples of such dependencies for six test images (the images Fr02, Fr03, and Fr04 are of approximately the same complexity as the test image Fr01 in Fig. 1, c) taken from the paper (Kovalenko et al., 2021) are presented in Fig. 2.

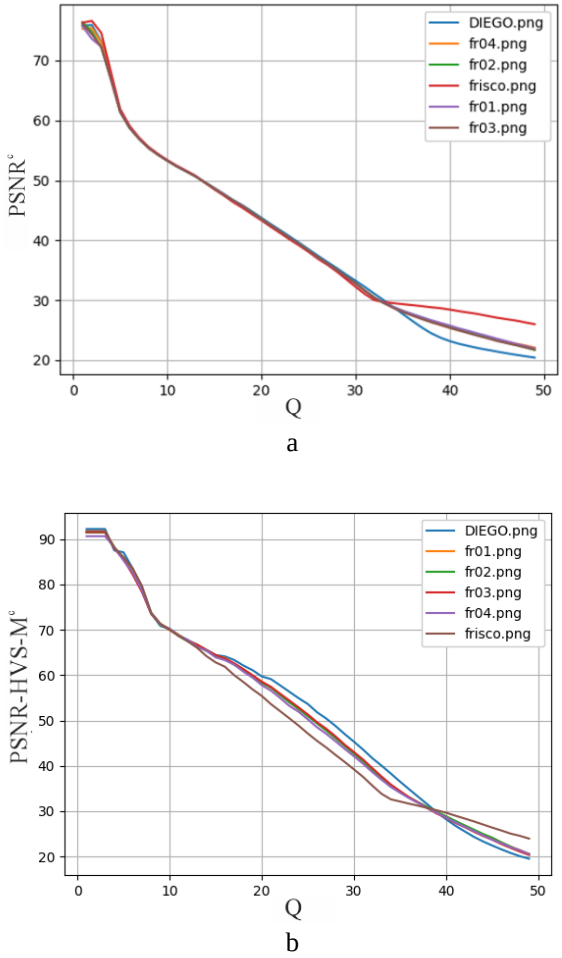

Fig. 2. Dependencies of PSNR and PSNR–HVS–M on Q for the coder BPG for six test images corrupted by AWGN with variance equal to 64 ($PSNR^n$ is about 30 dB)

As one can see, three main areas can be defined in these curves. The first is for Q < 9 where dependencies are nonlinear and quality of compressed images is characterized by very high values of $PSNR^c$ and $PSNR–HVS–M^c$ that mean that almost no distortions are introduced. Then, for Q from about 9 till Q = 33, one has practically linear reduction of $PSNR^c$ (approximately as 63-Q) and almost linear reduction of $PSNR–HVS–M^c$ (approximately as 83–1.33 Q). This part of the curves corresponds to invisible distortions (for Q about 28 and less) and visible distortions for Q > 28. Visible distortions relate to both noise filtering and information content degradation. The third area (Q > 33) is characterized by diversion in dependency behavior depending on image complexity.

Similar analysis has been carried out for several other values of the noise variance. The margins of the first area are practically unchanged. The right margin of the second area depends on noise variance. The value of Q for the right margin is approximately equal to $Q_{rm} = 63 – PSNR^n$. In practice, dependencies of $PSNR^c$ and $PSNR–HVS–M^c$ on Q can be obtained for any particular image, but the approximations given above can be used to determine the starting point.

Theoretically, i.e. in simulations when one has a noise-free image, adds AWGN to it, and applies lossy compression, it is also possible to calculate metrics between a compressed image and the corresponding noise-free one. Let us denote such metrics as $PSNR^{ct}$ and $PSNR–HVS–M^{ct}$. Examples of such dependencies on Q for six test images are presented in Fig. 3 and 4.

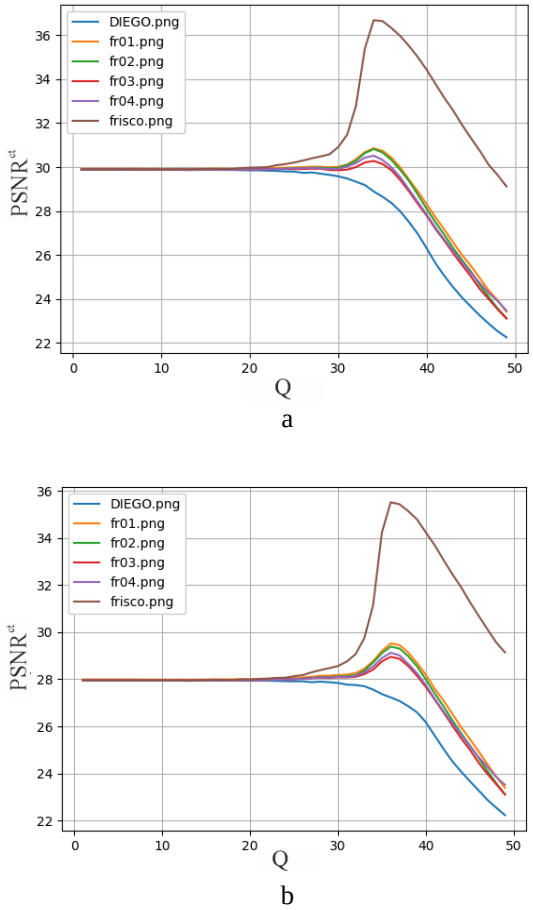

Fig. 3. Dependencies of $PSNR^{ct}$ on Q for the coder BPG for six test images corrupted by AWGN with variance equal to 64 (a, $PSNR^n$ is about 30 dB) and 100 (b, $PSNR^n$ is about 28 dB)

As one can see in Fig. 3, OOPs are observed for five out of six test images. For the simplest structure test image Frisco, OOP is more obvious than for other images. For the most complex structure image Diego, OOP is absent in both cases and the dependencies are monotonous. OOPs are “more obvious” for larger σ^2. Besides, Q for OOP is almost the same for all images for which OOP exists and it is larger for larger σ^2. Thorough analysis has shown that the formulas for Q_{OOP} can be written as $63\text{-}Q_{OOP} = PSNR^n$ or, equivalently,

$$Q_{OOP} = 14{,}9 + 20\log_{10}(\square\!\!\square\!\!\square\,\sigma). \quad (3)$$

Then, one has Q_{OOP} about 33 for σ = 8 (see data in Fig. 3, a) and about 35 for σ = 10 (see data in Fig. 3, b).

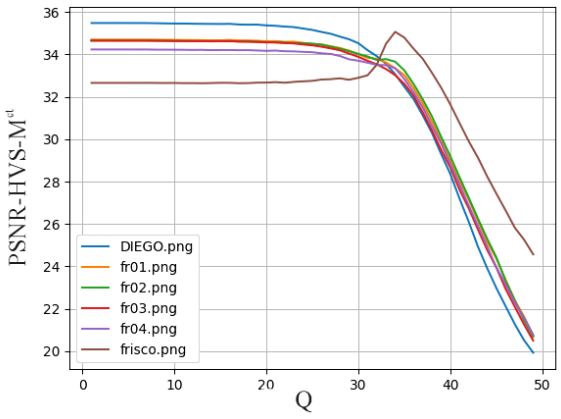

a

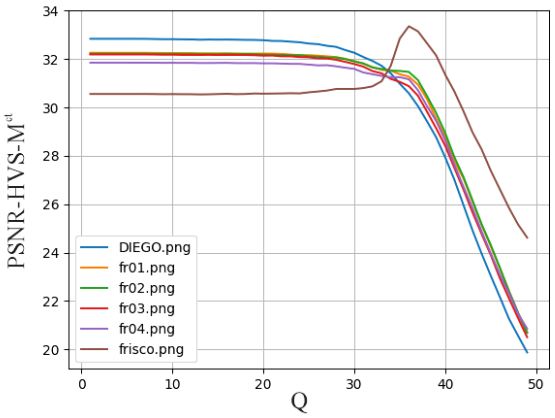

b

Fig. 4. Dependencies of PSNR–HVS–M^{ct} on Q for the coder BPG for six test images corrupted by AWGN with variance equal to 64 (a, $PSNR^n$ is about 30 dB) and 100 (b, $PSNR^n$ is about 28 dB)

Analysis of dependencies in Fig. 4 shows that OOP can be observed for visual quality metrics (e.g., PSNR–HVS–M) as well although this happens more rarely. OOP is not so "obvious" as for $PSNR^{ct}$. Expression (3) is approximately valid to determine Q_{OOP} according to this metric.

Summarizing the presented results and the data represented in the papers (Kovalenko et al., 2021 and Naumenko et al., 2021), it is possible to state that OOP can be observed and, if this happens, it is reasonable to compress such images in OOP. This allows providing compressed image quality closer to noise-free image compared to the original image and ensuring a rather large CR (Fig. 5 gives an example of such a situation). Meanwhile, if OOP does not exist for a given image, it is worth compressing this image with Q smaller than Q_{OOP} defined by (3) to avoid introducing too large distortions.

Thus, the task of predicting OOP existence for a given noisy image and quality parameters for OOP is important. Design of the corresponding method might allow carrying out automatic compression.

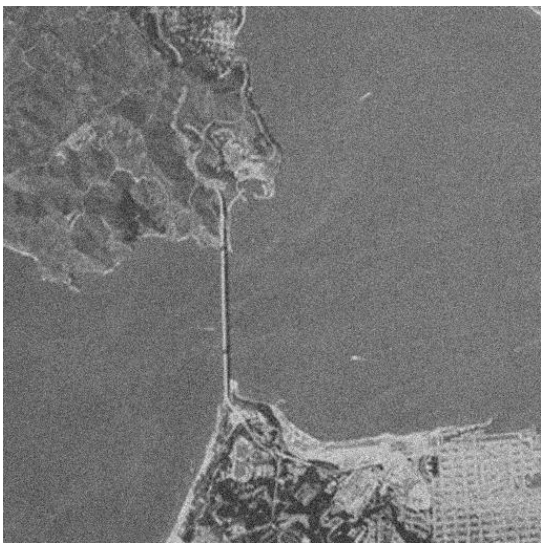

a

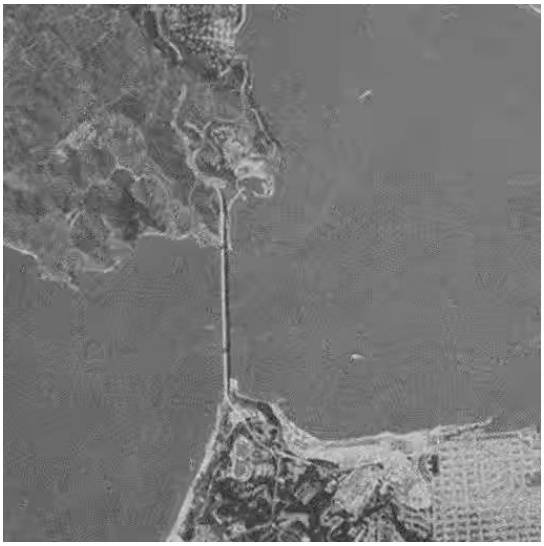

b

Fig. 5. Noisy image Frisco (a) and the same image compressed in OOP (b), noise variance equals to 196

3. Prediction of OOP existence and compression parameters in it

Formally, OOP exists if there is such Q that $Metr^{ct}(Q)$ is larger than $Metr^n$ where $Metr^{ct}$ is the full-reference metric calculated for the compressed and noise-free (true) image and $Metr^n$ is the same metric calculated between the noisy and true images (here we suppose that larger metric values correspond to better quality, this holds for both PSNR and PSNR–HVS–M as well as most other visual quality metrics). In practice, one does not have noise-free image and, therefore, neither $Metr^{ct}(Q)$ nor $Metr^n$ can be calculated. Because of this, we propose the following approach. We assume that it is possible to predict (estimate) the difference $\Delta M = Metr^{ct}(Q_{OOP}) - Metr^n$ keeping in mind that σ is a priori known or pre-estimated with high accuracy and, thus, Q_{OOP} is also known according to (3). Then, if a predicted ΔM is positive, the conclusion (decision) is that OOP (according to a considered metric) exists and vice versa.

In fact, we employ the approach similar to that one earlier proposed in the paper (Zemliachenko et al., 2015) for the DCT based coders and check whether or not it is applicable for the BPG coder.

3.1. Prediction approach

First, let us recall requirements to prediction. It should be fast enough and accurate enough. Saying fast, we mean that it has to be faster than compression itself. Saying accurate enough, it is meant that errors of ΔM prediction should have root mean square error (RMSE) small enough (e.g., less than 1 dB for the metrics PSNR and PSNR–HVS–M, both expressed in dB).

Generally speaking, the approach (Zemliachenko et al., 2015) presumes that there is a dependency between ΔM and some input parameter which "characterizes" image/noise properties and can be easily calculated. This dependency is known (determined) in advance (off line) and it is available to the moment when OOP existence has to be predicted for a given image to be compressed.

As input parameters, several statistical parameters have been proposed and tested in (Zemliachenko et al., 2015). They are based on comparison of amplitudes of DCT coefficients calculated in 8x8 pixel blocks to certain thresholds connected with noise standard deviation. Simplicity of obtaining such input parameters deals with two aspects. First, DCT in 8x8 pixels blocks is a standard operation in image/video processing (Wei et al., 2009) and it can be realized very quickly. Second, DCT should not be carried out for all possible block positions of a given image. It is enough to take 300…1000 randomly placed blocks to estimate the input parameter with appropriate accuracy (this will become clear later from analysis of scatter-plots).

It is unclear at the moment what statistical parameter of the considered type is the best for the analyzed application. We try to show only that the proposed approach is able to work quite well leaving the optimization task for the future research.

3.2. Scatter-plot obtaining and curve fitting

Similarly to the paper (Zemliachenko et al., 2015), we consider two input parameters – $P_{2\sigma}$ and $P_{2.7\sigma}$. The first parameter is the probability that DCT coefficient amplitudes are smaller than 2σ. The second parameter is the probability that DCT coefficient amplitudes are larger than 2.7σ. Such parameters have originated from the theory of DCT-based denoising (Abramov et al., 2013). Their properties will become clear from the further analysis.

To get prediction dependencies, scatter-plots of ΔM on input parameters have been obtained. One example is presented in Fig. 6 for ΔPSNR and $P_{2\sigma}$. Each particular point of the scatter-plot corresponds to one test image corrupted by AWGN with a given noise variance and compressed with Q_{OOP} set according to (3). We have used 11 test images of different complexity and 8 values of the noise variance in the limits from 0.25 to 400.

Analysis of data in Fig. 6 shows the following. First, $P_{2\sigma}$ varies in the wide limits from almost zero to almost unity. Small values of $P_{2\sigma}$ relate to complex structure images and/or rather small noise variances (see an example in Fig. 7, edge/detail smoothing is observed in the compressed image). In turn, large values of $P_{2\sigma}$ take place for simple structure images corrupted by a rather intensive noise (see the example in Fig. 5).

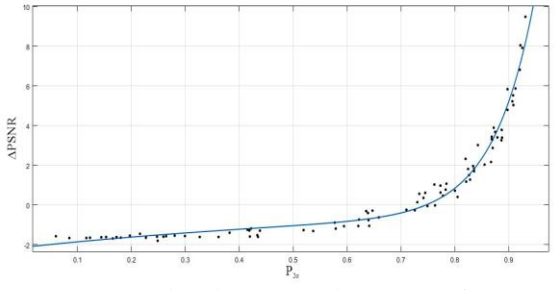

Fig. 6. The scatter-plot of ΔPSNR and $P_{2\sigma}$ and the fitted curve

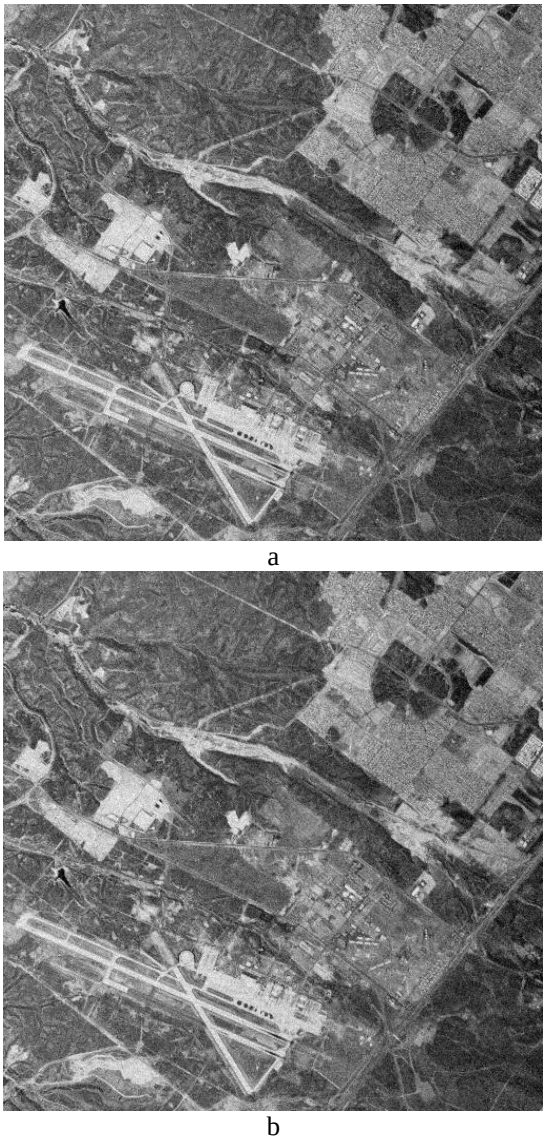

a

b

Fig. 7. Noisy image Diego (a) and the same image compressed in OOP (b), noise variance equals to 64

Second, ΔPSNR varies in rather wide limits from about –2 dB (see the data in Fig. 3, a for the test image Diego) till about +8 dB (see the data in Fig. 3, b for the test image Frisco).

Third, there is an obvious tendency to ΔPSNR increasing if $P_{2\sigma}$ becomes larger. Diversity of scatter-plot points for a given $P_{2\sigma}$ is not large (mostly smaller than 1 dB). This means that potentially accurate fitting is

possible and, using the fitted curves, it is possible to predict ΔPSNR quite accurately (in the next subsection, these questions will be discussed more in detail).

Fourth, if the main question is the OOP existence (but not prediction of ΔPSNR value in OOP), then a simple rule is possible. One can consider that OOP for the PSNR metric exists with rather high probability if $P_{2\sigma}$ exceeds 0.75.

Consider now another input parameter – $P_{2.7\sigma}$. The scatter-plot of ΔPSNR vs $P_{2.7\sigma}$ is presented in Fig. 8. In opposite to the scatter-plot in Fig. 8, there is a tendency of ΔPSNR reduction if $P_{2.7\sigma}$ increases. This is because $P_{2\sigma}$ and $P_{2.7\sigma}$ are defined in different ways (smaller and larger than the threshold, respectively). In this case, the rule for decision undertaking on OOP existence can be formulated as follows: OOP exists with high probability if $P_{2.7\sigma}$ is smaller than 0.15. Thus, decision can be undertaken for both input parameters.

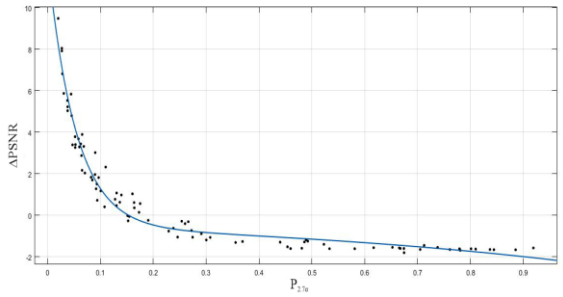

Fig. 8. The scatter-plot of ΔPSNR and $P_{2.7\sigma}$ and the fitted curve

Let us analyze now is it possible to predict ΔPSNR–HVS–M. The scatter-plots for ΔPSNR–HVS–M vs $P_{2\sigma}$ and $P_{2.7\sigma}$. are represented in Fig. 9. The scatter-plots are not so compact as for ΔPSNR. Meanwhile, the main tendencies are similar to those ones observed before. ΔPSNR–HVS–M increases if $P_{2\sigma}$ increases and $P_{2.7\sigma}$ reduces. OOP according to ΔPSNR–HVS-M is observed for a smaller number of images.

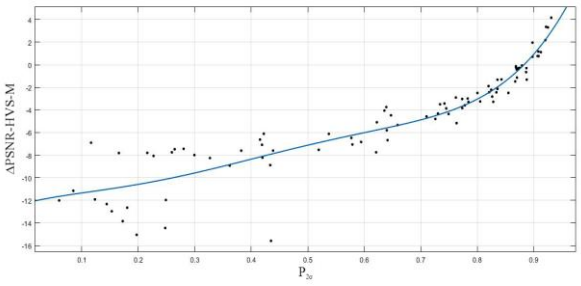

a

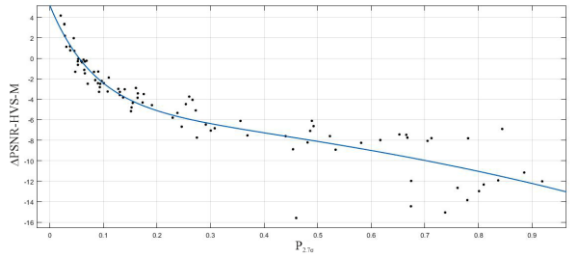

b

Fig. 9. The scatter-plot of ΔPSNR–HVS–M vs $P_{2\sigma}$ (a) and $P_{2.7\sigma}$ (b) and the fitted curves

One specific feature is that ΔPSNR–HVS–M varies in other limits than ΔPSNR: from about –15 dB to about 4 dB. According to ΔPSNR–HVS–M, OOP is observed if $P_{2\sigma}$ exceeds 0.85 or $P_{2.7\sigma}$ is less than 0.08.

It might seem that a very large reduction of PSNR–HVS–M^{ct} due to lossy compression can be observed (as it follows from the scatter-plots in Fig. 9, ΔPSNR–HVS–M can be about –10 dB). However, it is not a fatal case – this happens for $P_{2\sigma}$ about 0.2 ($P_{2.7\sigma}$ about 0.7), i.e. for very complex images with low intensity noise. This means that PSNR–HVS–M^{n} can be of the order 60 dB and PSNR–HVS–M^{ct} for Q_{OOP} is 50 dB. PSNR–HVS–M^{n} about 60 dB means that noise is invisible in original image and PSNR–HVS–M^{ct} about 50 dB means that introduced distortions are not visible too. Thus, ΔPSNR–HVS–M about –10 dB in such cases is not a problem. The problem is if PSNR–HVS–M^{n} is about 30–40 dB (i.e., noise is visible) and ΔPSNR–HVS–M is about –2 dB. Just such cases take place for the test image Diego in Fig. 4, the illustration is given in Fig. 7.

3.3. Curve fitting and prediction accuracy

We have not yet studied the question of curve fitting into scatter-plots. On one hand, the examples shown in Fig. 6, 8, and 9 intuitively show that fitting can be done efficiently. On the other hand, requirements to fitting and quantitative criteria of fitting efficiency have not been discussed.

The curve fitting into a scatter-plot can be done by different methods, using different tools and criteria (Cameron et al., 1997 and Guruswami et al., 2016). In particular, Matlab and Excel offer good facilities for curve fitting. In our studies, we have used Matlab Curve Fitting Tool.

Fitting quality is usually characterized by several quantitative parameters (criteria) such as goodness-of-the-fit R^2, RMSE, Adjusted R^2 and so on (Cameron et al., 1997). R^2 and Adjusted R^2 have to be as large as possible (approaching to unity) and RMSE should be as small as possible for good fitting. The regression is considered very good if R^2 and Adjusted R^2 exceed 0.9.

In (Zemliachenko et al., 2015), polynomial approximation has been used. It has been shown that polynomials of the fourth and fifth order usually provide good fitting. Two examples of polynomial fitting are given in Fig. 10. For the data in Fig. 10, a, one has $R^2 = 0.93$, RMSE = 0.71, Adjusted $R^2 = 0.93$, i.e. the results are quite good. For the fifth order polynomial (Fig. 10, b), the fitting results are even better ($R^2 = 0.97$, RMSE = 0.47, Adjusted $R^2 = 0.97$). Meanwhile, the fitted curves are not monotonous and local maxima can be observed. We do not state that the dependencies should be monotonous but it seems so from visual analysis of the scatter-plots.

Rather good polynomial fitting results have been obtained for the scatter-plot of ΔPSNR–HVS–M vs $P_{2\sigma}$ (see Fig. 11). The obtained curves for all polynomials are monotonous and the best fitting has been obtained for the fifth order polynomial ($R^2 = 0.87$, RMSE = 1.66, Adjusted $R^2 = 0.86$). Note that large RMSE is mainly due to diversity of scatter-plot data for $P_{2\sigma} < 0.5$. This does not sufficiently influence the decision on OOP existence.

Meanwhile, the fitting results are worse than for the scatter-plots of ΔPSNR vs $P_{2\sigma}$. The reason is that the scatter-plot of ΔPSNR–HVS–M vs $P_{2\sigma}$ is not as compact as the scatter-plot of ΔPSNR–HVS–M vs $P_{2\sigma}$.

Analysis carried out for the scatter-plots where $P_{2.7\sigma}$ was used as the argument has shown that fitting for each particular case is slightly worse than for $P_{2\sigma}$. For example, for the fifth order polynomial for the scatter-plot ΔPSNR vs $P_{2.7\sigma}$ one has $R^2 = 0.95$, RMSE = 0.62, Adjusted $R^2 = 0.95$. This allows coming to preliminary conclusion that it is worth using $P_{2\sigma}$ as input parameter.

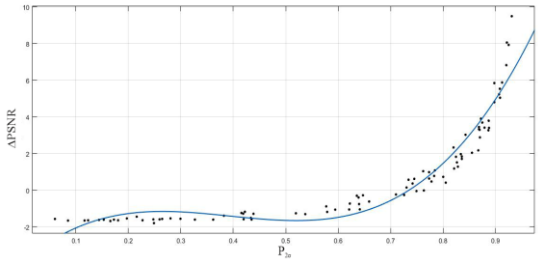

a

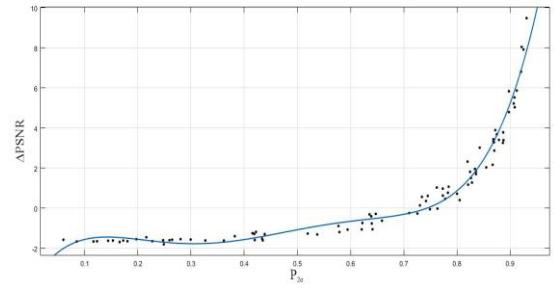

b

Fig. 10. Examples of polynomial fitting for ΔPSNR vs $P_{2\sigma}$ for polynomials of the third (a) and fifth (b) orders

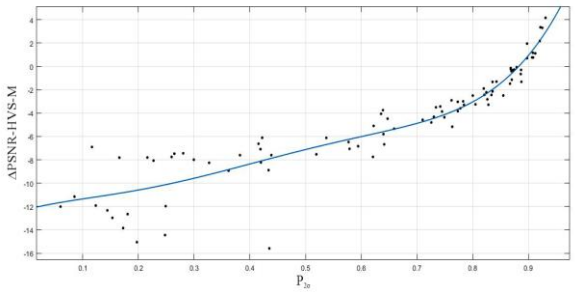

Fig. 11. Example of polynomial fitting for ΔPSNR–HVS–M vs $P_{2\sigma}$ for polynomials of the fifth order

It is worth stressing that polynomial-based fitting is not the only possible option. In particular, another option is to use a sum of two exponents as

$$f(x) = a * \exp(bx) + c * \exp(dx), \quad (4)$$

where there are four adjustable parameters: *a*, *b*, *c*, and *d*. Just such fitting functions with adjusted parameters are shown in Fig. 6, 8, and 9. Visually, fitting is very good and the obtained curves are monotonous. Let us also analyze quantitative characteristics. They are given in Table 1. As one can see, the conclusions that can be drawn are the same as for polynomial fitting. The use of $P_{2\sigma}$ as input parameter provides slightly better fitting than the use of $P_{2.7\sigma}$. ΔPSNR–HVS–M is approximated and, thus, predicted worse than ΔPSNR.

Table 1. Fitting characteristics for the sums of two exponents

Predicted parameter	Input parameter	R^2	Adjusted R^2	RMSE
ΔPSNR	$P_{2\sigma}$	0.974	0.973	0.437
ΔPSNR	$P_{2.7\sigma}$	0.963	0.962	0.523
ΔPSNR–HVS–M	$P_{2\sigma}$	0.870	0.865	1.64
ΔPSNR–HVS–M	$P_{2.7\sigma}$	0.863	0.859	1.68

Keeping in mind the monotonicity of the approximation (4) and its accuracy characteristics, we recommend using the following approximations:

$$\Delta\text{PSNR} = 0.0008269 * \exp(9.755 * P_{2\sigma}) - \\ - 13.24 * \exp(-1.192 * P_{2\sigma}). \quad (5)$$

$$\Delta\text{PSNR–HVS–M} = -4.897 * \exp(-4.897 * P_{2\sigma}) + \\ + 10.07 * \exp(-12.12 * P_{2\sigma}). \quad (6)$$

Above, we have paid attention to accuracy of approximations meaning that they determine accuracy of prediction. This is, in general, true although accuracy of prediction is also determined by one more factor, namely, how accurately input parameters are estimated. Special study has shown that $P_{2\sigma}$ for most images can be determined with errors less than 0.01 if the number of analyzed blocks is of the order 300–1000. As it follows from analysis of the fitted curves' behavior, such errors usually do not lead to essential changes (systematic errors) of predicted values. At least, such errors are smaller than RMSE.

Finally, other functions can be used in scatter-plot fitting. This can be a direction of the future studies.

4. Conclusions and future work

In this paper, we have shown that BPG-based lossy compression of noisy images has specific features. In particular, OOP can be observed under condition that an image is quite simple and noise is quite intensive. If OOP exists, it is reasonable to compress a given image in OOP. If OOP is not observed, Q should be set smaller than Q_{OOP} not to introduce too large distortions.

It is also demonstrated that it is possible to predict does OOP exists and, moreover, what is image quality for Q_{OOP}. Possibility of OOP existence is shown for two metric and this can be done quite easily and quickly. The prediction employs simple analysis of DCT coefficient statistics determined in a limited number of 8x8 pixel blocks. Having this prediction, it becomes possible to undertake a correct decision what Q to set.

In the future, we plan to consider the cases of signal dependent noise and multichannel images. Maybe, prediction accuracy for the metric PSNR–HVS–M can be improved.

References

Abramov S., Krivenko S., Roenko A., Lukin V., Djurović I. and Chobanu M. (2013). Prediction of filtering efficiency for DCT-based image denoising. *2013 2nd Mediterranean Conference on Embedded Computing (MECO)*, 97–100. DOI: 10.1109/MECO.2013.6601327.

Aiazzi B., Alparone L., Baronti S., Lastri C., Selva M. (2012). Spectral distortion in lossy compression of hyperspectral

data. *Journal of Electrical Computer Engineering*, Article ID 850637, 8. DOI: https://doi.org/10.1155/2012/850637.

Albalawi U., Mohanty S. P. and Kougianos E. (2016). Energy-Efficient Design of the Secure Better Portable Graphics Compression Architecture for Trusted Image Communication in the IoT. *2016 IEEE Computer Society Annual Symposium on VLSI (ISVLSI)*, 302–307. DOI: 10.1109/ISVLSI.2016.21.

Al-Shaykh O. K., Mersereau R. M. (1998). Lossy compression of noisy images. *IEEE Transactions on Image Processing*, 7(12), 1641–1652. DOI: 10.1109/83.730376.

Bataeva E. V. (2012). Flanering and video mania: Modern and postmodern visual practices. *Voprosy Filosofii*, 11, 61–68.

Bondžulić B., Stojanović N., Petrović V., Pavlović B., Miličević Z. (2021). Efficient Prediction of the First Just Noticeable Difference Point for JPEG Compressed Images. *Acta Polytechnica Hungarica*, 18(8), 201–220. DOI: 10.12700/APH.18.8.2021.8.11

Braunschweig R., Kaden I., Schwarzer J., Sprengel C., Klose K. (2009). Image data compression in diagnostic imaging: International literature review and workflow recommendation. *Rofo*, 181(7), 629–636.

Cameron A. C. and Windmeijer F. (1997). An R-squared measure of goodness of fit for some common nonlinear regression models. *Journal of Econometrics*, 77(2), 329–342. DOI: 10.1055/s-0028-1109341.

Chang S. G., Yu B., Vetterli M. (1997). Image denoising via lossy compression and wavelet thresholding. *Proceedings of International Conference on Image Processing*, 1, 604–607. DOI: 10.1109/ICIP.1997.647985.

Chatterjee P. and Milanfar P. (2010). Is Denoising Dead? In *IEEE Transactions on Image Processing*, 19(4), 895-911. DOI: 10.1109/TIP.2009.2037087.

Chi M., Plaza A., Benediktsson J. A., Sun Z., Shen J., Zhu Y. (2016). Big data for remote sensing: Challenges and opportunities. *Proceedings of the IEEE*, 104(11), 2207–2219. DOI: 10.1109/JPROC.2016.2598228.

Christophe E. (2011). Hyperspectral Data Compression Tradeoff. In: *Prasad S., Bruce L., Chanussot J. (eds) Optical Remote Sensing. Augmented Vision and Reality*. DOI: 10.1007/978-3-642-14212-3_2.

Colom M., Buades A., Morel J.-M. (2014). Nonparametric noise estimation method for raw images. *J. Opt. Soc. Am.*, 31(4), 863–871. DOI: 10.1364/JOSAA.31.000863.

Doss S., Pal S., Akila D., Jeyalaksshmi S., Jabeen T. N., Suseendran G. (2020). Satellite image remote sensing for identifying aircraft using SPIHT and NSCT. *IEEE Signal processing magazine*, 7(5), 631–634.

Guruswami V., Zuckerman D. (2016). Robust Fourier and Polynomial Curve Fitting. *2016 IEEE 57th Annual Symposium on Foundations of Computer Science (FOCS)*, 751–759. DOI: 10.31838/jcr.07.05.130.

Hussain A. J., Al-Fayadh A., and Radi N. (2018). Image compression techniques: A survey in lossless and lossy algorithms. *Neurocomputing*, 300, 44–69. DOI: 10.1016/j.neucom.2018.02.094.

Kovalenko B., Lukin V., Naumenko V., Krivenko S. (2021). Analysis of noisy image lossy compression by BPG using visual quality metrics. *2021 IEEE 3rd International Conference on Advanced Trends in Information Theory (ATIT)*, 20–25. DOI: 10.1109/ATIT54053.2021.9678575.

Khorram S., van der WieleFrank C. F., Koch F. H., Nelson S. C., Potts M. D. (2016). Future Trends in Remote Sensing. *Principles of Applied Remote Sensing*, 277–285.

Krivenko S., Lukin V., Krylova O. (2019). Visually Lossless Compression of Dental Images. *2019 IEEE 39th International Conference on Electronics and Nanotechnology (ELNANO)*, 394–399.

Li F., Krivenko S., Lukin V. (2020). Adaptive two-step procedure of providing desired visual quality of compressed image. *Proceedings of the 2020 4th International Conference on Electronic Information Technology and Computer Engineering*, 407–414. DOI: 10.1145/3443467.3443791.

Li F., Krivenko S., Lukin V. (2020). A Fast Method for Visual Quality Prediction and Providing in Image Lossy Compression by SPIHT. *Proceedings of Conference on Integrated Computer Technologies in Mechanical Engineering–Synergetic Engineering*, 17–29. DOI: 10.1007/978-3-030-66717-7_2.

Ma Y., Wu H., Wang L., Huang B., Ranjan R., Zomaya A., Jie W. (2015). Remote sensing big data computing: Challenges and opportunities. *Future Generation Computer Systems*, 51, 47–60. DOI: 10.1016/j.future.2014.10.029.

Mahanti N. K., Pandiselvam R., Kothakota A., Ishwarya P., Chakraborty S. K., Kumar M., Cozzolino D. (2021). Emerging non-destructive imaging techniques for fruit damage detection: Image processing and analysis. *Trends in Food Science & Technology*, 120, 418–438. DOI: 10.1016/j.tifs.2021.12.021.

Naumenko V., Lukin V., Krivenko S., Kovalenko B. (2021). Lossy compression of single-channel images corrupted by additive white noise with performance prediction. Accepted to ICTM, 2021.

Pandey A., Saini B. S., Singh B., Sood N. J. M. (2020). Quality controlled ECG data compression based on 2D discrete cosine coefficient filtering and iterative JPEG2000 encoding. *Measurement*, 152, 107252. DOI: 10.1016/j.measurement.2019.107252.

Penna B., Tillo T., Magli E., Olmo G. (2007). Transform coding techniques for lossy hyperspectral data compression. *IEEE Transactions on Geoscience Remote Sensing*, 45(5), 1408–1421. DOI: 10.1109/TGRS.2007.894565.

Ponomarenko N., Lukin V., Astola J., Egiazarian K. (2015). Analysis of HVS-metrics' properties using color image database TID2013. In *International Conference on Advanced Concepts for Intelligent Vision Systems*, 613–624. DOI: 10.1007/978-3-319-25903-1_53.

Ponomarenko N., Silvestri F., Egiazarian K., Carli M., Astola J., Lukin V. (2007). On between-coefficient contrast masking of DCT basis functions. *Proceedings of the Third International Workshop on Video Processing and Quality Metrics for Consumer Electronics*, 4.

Said A., Pearlman W. A. (1996). A new, fast, and efficient image codec based on set partitioning in hierarchical trees. *IEEE Transactions on Circuits and Systems for Video Technology*, 6(3), 243–250. DOI: 10.1109/76.499834.

Sayood K. (2017) Introduction to data compression, San Francisco: Morgan Kaufmann, 768. ISBN: 978-0-12-415796-5

Selva E., Kountouris A., Louet Y. (2021). K-Means Based Blind Noise Variance Estimation. *2021 IEEE 93rd Vehicular Technology Conference (VTC2021-Spring)*, 1–7. DOI: 10.1109/VTC2021-Spring51267.2021.9449072.

Tao D., Di S., Liang X., Chen Z., Cappello F. (2018). Fixed-PSNR Lossy Compression for Scientific Data. *2018 IEEE International Conference on Cluster Computing (CLUSTER)*, 314-318. DOI: 10.48550/arXiv.1805.07384.

Taubman D. S., Marcellin M. W. (2013). *JPEG2000: image compression fundamentals, standards, and practice*. Retrived from http://extras.springer.com. DOI: 10.1007/978-1-4615-0799-4.

Wang Z., Simoncelli E. P., Bovik A. C. (2003). Multiscale structural similarity for image quality assessment. *IEEE Asilomar Conference on Signals, Systems and Computers*, 2, 1398–1402. DOI: 10.1109/ACSSC.2003.1292216.

Wei Z., Ngan K. N. (2009). Spatio-Temporal Just Noticeable Distortion Profile for Grey Scale Image/Video in DCT Domain. *IEEE Transactions on Circuits and Systems for*

Video Technology, 19(3), 337–346. DOI: 10.1109/TCSVT.2009.2013518.

Yee D., Soltaninejad S., Hazarika D., Mbuyi G., Barnwal R. and Basu A. (2017). Medical image compression based on region of interest using better portable graphics (BPG). *2017 IEEE International Conference on Systems, Man, and Cybernetics (SMC)*, 216–221. DOI: 10.1109/SMC.2017.8122605.

Zabala A., Pons X., Diaz-Delgado R., Garcia F., Auli-Llinas F. and Serra-Sagrista J. (2006). Effects of JPEG and JPEG2000 Lossy Compression on Remote Sensing Image Classification for Mapping Crops and Forest Areas. *2006 IEEE International Symposium on Geoscience and Remote Sensing*, 790–793. DOI: 10.1109/IGARSS.2006.203.

Zappavigna M. (2016). Social media photography: construing subjectivity in Instagram images. *Visual Communication*, 15(3), 271–292. DOI: 10.1177/1470357216643220.

Zemliachenko A., Abramov S., Lukin V., Vozel B., Chehdi K. (2015). Lossy Compression of Noisy Remote Sensing Images with Prediction of Optimal Operation Point Existence and Parameters. *SPIE Journal on Advances in Remote Sensing*, 9(1), 26. DOI: 10.1117/1.JRS.9.095066.

Zhai G., Min X. (2020). Perceptual image quality assessment: a survey. *Science China Information Sciences*, 63, 1–52.

ПРОГНОЗУВАННЯ ПАРАМЕТРІВ В ОПТИМАЛЬНІЙ РОБОЧІЙ ТОЧЦІ ДЛЯ СТИСНЕННЯ З ВТРАТОЮ ЗОБРАЖЕНЬ З ШУМОМ НА ОСНОВІ BPG

Б. В. Коваленко[1], В. В. Лукін[1], С. С. Кривенко[1], В. В. Науменко[1], Б. Возель[2]

[1] *Національний аерокосмічний університет, кафедра інформаційно-комунікаційних технологій, Харків 61070, Україна*

[2] *IETR, UMR CNRS 6164, Університет м. Рен 1, 22305, Ланьйон, Франція*

Стиснення з втратою зображень, спотворених шумом, має декілька особливостей. По-перше, спостерігається специфічний ефект фільтрації шуму. По-друге, може спостерігатися оптимальна робоча точка (ОРТ), тобто може існувати таке значення параметра кодера (наприклад, кроку квантування), що якість стисненого зображення, розрахованого відносно безшумного зображення, може бути кращою порівняно з якістю стисненого (вихідного зашумленого) зображення. Якщо ОРТ є, то варто стиснути це зображення в ОРТ, якщо ні, то слушні інші рекомендації щодо налаштування параметрів кодера. Оскільки безшумне зображення на практиці недоступне, визначити, чи існує ОРТ і яка в ньому якість зображення, неможливо. У цій статті викладено, що існування ОРТ для кількох метрик якості можна досить легко і швидко прогнозувати для зображень у градаціях сірого, спотворених адитивним білим гауссовим шумом та стиснутим кодером better portable graphics (BPG). Такий прогноз ґрунтується на аналізі статистики коефіцієнтів дискретного косинусного перетворення (ДКП), розрахованих для обмеженої кількості блоків 8x8 пікселів. Діаграма розсіювання покращення (погіршення) метрики залежно від цих статистичних даних отримується заздалегідь і виконується підбір прогнозної кривої. Наведено рекомендації щодо налаштування параметрів кодера для випадків відсутності ОРТ.

Ключові слова: стиснення зображення із втратами, оптимальна точка роботи, якісне прогнозування, шум, дискретне косинусне перетворення.

Рукопис статті отримано 17.05.2022